Progress In Electromagnetics Research B, Vol. 65, 35–48, 2016

An Iterative Shrinkage Deconvolution for Angular Super-Resolution Imaging in Forward-Looking Scanning Radar

Yuebo Zha*, Yulin Huang, and Jianyu Yang

Abstract—The aim of angular super-resolution is to surpass the real-beam resolution. In this paper, a method for forward-looking scanning radar angular super-resolution imaging through a deconvolution method is proposed, which incorporates the prior information of the target's scattering characteristics. We first mathematically formulate the angular super-resolution problem of forward-looking scanning radar as a maximum a posteriori (MAP) estimation task based on the forward model, and convert it to an equivalent unconstrained optimization problem by applying the log-transforms to the posterior probability, which guarantees the solution converges to a global optimum of an associated MAP problem and it is easy to implement. We then implement the unconstrained optimization task in convex optimization framework using an iterative shrinkage method, and the computational complexity of the proposed algorithm is also discussed. Since the anti log-likelihood of the noise distribution and the prior knowledge of the scene are utilized, the proposed method is able to achieve angular super-resolution imaging in forward-looking scanning radar effectively. Numerical simulations and experimental results based on real data are presented to verify that the proposed deconvolution algorithm has better performance in preserving angular super-resolution accuracy and suppressing the noise amplification.

1. INTRODUCTION

With a non-coherent working mode, forward-looking scanning radar plays an important role in remote sensing and has been widely used in civilian and military fields. According to the principle of high-resolution radar [1], the upper limit of the radar real-beam angular resolution is determined by the wavelength and the antenna aperture. For an forward-looking scanning radar with fixed working frequency, to obtain a high angular resolution, a large antenna aperture is needed. However, there is a great challenge to accommodate the antenna with large size when the scanning radar is mounted on an airborne platform. Therefore, to improve the angular resolution of a real-beam scanning radar beyond the theoretically physical limit using deconvolution techniques is important. A number of papers on devonvolution algorithms such as image reconstruction [2], receiver-function estimation [3], sparse signal restoration [4] and super-resolution in radar [5–7] have been reported. However, less work on deconvolution algorithm for angular super-resolution imaging in scanning radar has been done. This paper aims at the deconvolution algorithm for angular super-resolution imaging in forward-looking scanning radar.

Under the Born hypothesis [8], the radar echo signal after range compression and range cell migration can be modeled as the convolution of the transmitting signals and the reflectivity of the illuminated scene. Therefore, deconvolution methods can enhance the angular resolution of real beam in theory [9, 10]. Convolution corresponds to multiplication in the Fourier domain while deconvolution is essentially Fourier division. Deconvolution is an effective approach for forward-looking scanning radar

Received 5 October 2015, Accepted 19 December 2015, Scheduled 2 January 2016

* Corresponding author: Yuebo Zha (zhayuebo@163.com).

The authors are with the School of Electronic Engineering, University of Electronic Science and Technology of China, 2006 Xiyuan Road, Gaoxin Western District, Chengdu 611731, China.

imaging, which is able to break through the theoretical limit of radar angular resolution. For a radar system, the output is the low-pass-filtered version of the original data due to the finite size of the antenna. The portions of the scenes lost through the antenna are the high-frequency components that accurately describe the objects in the scene and are crucial for the resolution of the radar image. There are many deconvolution algorithms to improve the angular resolution of real beam beyond the classical limit by incorporating the statistical characteristics of prior information about scenes [11, 12].

Basically, there are two main categories of deconvolution techniques: regularization theory and Bayesian approach. The core of the first one is modeling the unknowns as a deterministic function [13]. However, there are some certain shortcomings in this approach. First, errors considered in this approach are Gaussian noise and limited prior information is available for the solution. In addition, it is difficult to select the regularization parameter, which is very important to the solution of the deconvolution problem. In a nonlinear deconvolution framework, this task becomes rather difficult [14]. Using Bayesian deconvolution approaches, we can make use of statistical prior information of the scenes. Hence, we focus on the Bayesian approach to solve the deconvolution problem in this paper.

In Bayesian deconvolution approaches, the unknown parameters are modeled as stochastic variables, and the probability density functions are assigned to them, respectively [15, 16]. In this framework, we can formulate the prior information of the data, which is ignored in the regularization methods. The specific prior information we use includes not only the statistical characteristics of the target backscatter coefficients but also the statistical characteristics of the noise, which can be expressed as probability density functions. Another important advantage of Bayesian approach over the regularization theory is that the Bayesian approaches are based on mathematical models, and they can handle observation noise and missing data problems. One popular deconvolution algorithm in Bayesian framework is Richardson-Lucy (R-L) deconvolution algorithm [17, 18]. This algorithm does not converge to the solution because the noise is amplified during the deconvolution process due to the ill-posed nature of the deconvolution problem. The conventional approach to suppress noise amplification is to stop the iteration when the result of deconvolution becomes too noisy. However, it is difficult to decide when to stop the iteration [19]. To overcome this drawback, it was proposed in [20] to replace the maximum likelihood (ML) approach by maximum a posterior (MAP) estimator via incorporating the prior knowledge of the unknown objects.

In this paper, we propose an approach to solve the deconvolution problem from a perspective of Bayesian framework. The Laplace distribution is employed to formulate the prior information of the objects, which represents the statistical characteristics of strong scatters' distribution in the illuminated scene. In the framework of Bayesian theory, the problem of forward-looking scanning radar imaging with angular super-resolution is converted into MAP problem mathematically, which is well suited to this application since it is directly expressed using the likelihood function of the noise and the prior knowledge of the scene and therefore does not require any approximation. Then, we convert the MAP problem into an equivalent unconstrained optimization task using the logarithm. As will be shown, this transformation results in a regularization term, which is of difficult when solving the corresponding unconstrained optimization problem due to the non-differentiability of negative log-prior around the original. We solve the unconstrained optimization problem using the iterative shrinkage approach [21–24], with the superiority not only in guaranteeing the optimal solution of unconstrained optimization problem converged to the global optimal solution but also in obtaining the angular super-resolution with high precision. Experimental results with synthetic and real data illustrate that the proposed algorithm provides competitive and higher angular super-resolution performance.

The rest of the paper is organized as follows. The geometry model and signal model of forward-looking scanning radar imaging are described in Section 2. In Section 3, we discuss the inverse problem, including the Bayesian inversion for deconvolution problems, an iterative shrinkage algorithm, computational complexity and the selection of regularization parameter. In Section 4, the proposed deconvolution algorithm is compared with the conventional Richardson-Lucy deconvolution algorithm in terms of super-resolution performance on synthetic and real data. Finally, we draw our conclusions in Section 5.

2. PROBLEM FORMULATION

In this section, we present the geometry model of the forward-looking scanning radar and its signal model.

2.1. Geometry Model

The geometry model of forward-looking scanning radar imaging is illustrated in Fig. 1(a). Suppose that the radar works in forward-looking scan mode. The radar platform moves at a constant velocity V in the flight path along the axis X and the antenna beam scans with a constant angular velocity ω along the axis Y. In the Fig. 1, X represents the range dimension and Y denotes the azimuth dimension. The antenna beam scans the scene and receives the echo reflected from the observed scene. The process of receiving echo data is shown in the upper part of Fig. 1, which is termed forward model.

In the forward-looking scanning radar system, high range resolution can be obtained by maximum autocorrelation. However, it is impossible to achieve high azimuth or angular resolution in the front area of the scanning radar by maximum autocorrelation, because the direction of Doppler resolution and range resolution are the same. Therefore, an effective imaging algorithm for high angular resolution in the forward-looking area of radar is desired. Deconvolution provides a new thinking to develop forward-looking scanning radar imaging techniques with high angular resolution, but little work on the use of deconvolution techniques for forward-looking scanning radar angular super-resolution imaging has been reported. Aiming to provide a deconvolution approach for forward-looking scanning radar imaging with angular super-resolution, the range compression and range cell migration are applied to the echo data beforehand. In radar angular super-resolution imaging applications, according to the Born hypothesis, the echo data after range compression and range cell migration can be modeled as the convolution of the antenna with the reflectivity of the observed scene.

2.2. Signal Model

The signal through range compression and range cell migration processing is denoted by $g(\tau, \eta)$, shown in Fig. 1(d). Under the Born hypothesis, it can be assumed that the $g(\tau, \eta)$ after range compression and range cell migration can be modeled as the convolution of the antenna beam $h(\tau, \eta)$ with the reflectivity of the observed scene $f(\eta)$. That is

$$g(\tau, \eta) = \int_{-\infty}^{+\infty} h(\tau, \eta - \eta') f(\eta') d\eta' + n(\tau, \eta) \tag{1}$$

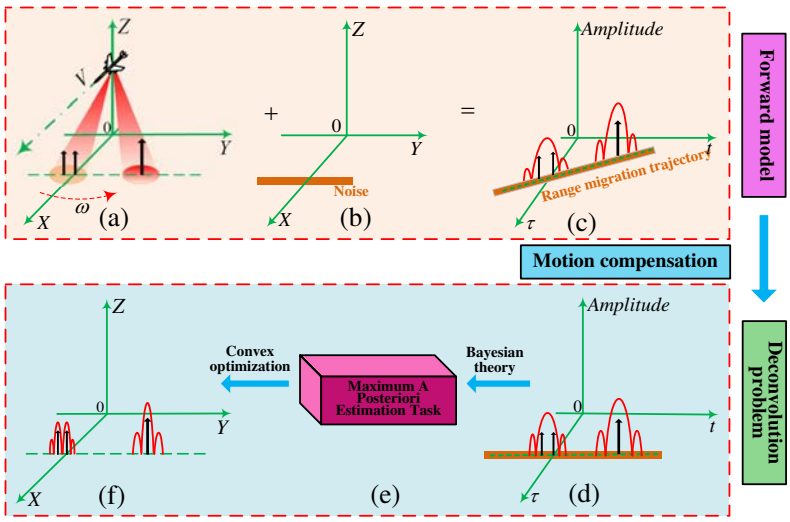

Figure 1. Diagram of forward-looking scanning radar imaging model.

where τ represents the fast time, η the slow time and $n(\tau, \eta)$ the noise.

In the case of imaging a certain scene Ω, let $g(\tau_i, \eta_j)$ be the i-th fast time sample at j-th observation of echo $g(\tau, \eta)$ and let $f(x_m, y_n)$ be the discrete backscattering coefficient at m-th position of the range dimension and n-th position along the azimuth dimension of the observation scene. Then, we can rewrite the (1) as

$$g(\tau_i, \eta_j) = \sum_{m=1}^{M_a} \sum_{n=1}^{M_r} h(i, j, m, n) f(x_m, y_n) + N(\tau_i, \eta_j). \tag{2}$$

where M_a denotes the number of discrete cells in angular direction; M_r is number of the discrete cells of scene in range direction. After range compression and range cell migration applied to the echo data, the signal is denoted by g. Then, the data g can be represented as a vector $g = [g_1, g_2, \ldots g_{N_r \cdot N_a}]^T$ (same for f and n) by stacking all the $N_r \cdot N_a$ the data into a vector in lexicographic order, where N_r and N_a denote the discrete point numbers along the fast and slow time dimensions, respectively.

Then, we obtain the following forward model of airborne forward-looking scanning radar imaging

$$g = Hf + n. \tag{3}$$

where f is the unknown true scene with the size of $(M_a \cdot M_r) \times 1$, whose pixel values are corresponding to scattering center's amplitudes. n is the noise vector with the same size as g. The matrix H is of the size $(N_a \cdot N_r) \times (M_a \cdot M_r)$, which represents the response matrix. The role of matrix H can also be interpreted as a map from the discrete domain of the observed scene to the space of the recorded radar echo data.

The lower right corner of Fig. 1 shows the echo data after range compression and range cell migration in forward-looking scanning radar, which is described by (3). In the Fig. 1, the illuminated scene consists of three targets, of which two are closely spaced in range. The targets are of unequal heights. The beam of forward-looking scanning radar scans in azimuth across the target field. Range compression and range cell migration have been used to the echo data, and the resulting signal is shown in the lower-right of Fig. 1, which is denoted as g. For an isolated target, the amplitude of the received signal at the receiver output is proportional to the antenna pattern and it is isolated from the other two targets. For two targets closely spaced in range, the response of these targets is proportional to two replicas of the antenna pattern, overlapped and added to get a composite response. In this case, the individual response is not resolved, but together form a single peak. The resulting low-resolution signal is illustrated in the lower right corner of Fig. 1.

At this point, the goal of forward-looking scanning radar imaging with angular super-resolution is to infer f, as accurately as possible, from the samples g. This task is called inverse problem in this paper. It is the fact that the convolution corresponds to multiplication in the Fourier, while deconvolution refers to Fourier division. For radar system, we should note that data g recorded at the output of the system is a low-pass filtered version of the original scene f because of the band-limited character of antenna pattern in the angular frequency domain. The multipliers are often small for high frequencies, and direct division is unstable and plagued by noise existed in the input data. Therefore, the original scene f reconstructed from g via conventional inverse filters can not work because the conventional inverse filter magnifies the components that has low signal-to-noise ratios in an attempt to restore high frequencies, thus magnifies the noise much more. This phenomenon is defined as ill-posed.

To make use of the deconvolution algorithm for forward-looking scanning radar imaging with angular super-resolution, one must transform the original ill-posed problem to a 'nearby' well-conditioned problem whose solution approximates the required solution. To reach this aim, we convert the angular super-resolution problem into an equivalent MAP estimation task, which enables us to add some prior information to compensate the missing high frequencies data. Then, we solve the corresponding MAP estimation task within the framework of convex optimization. The lower part of Fig. 1 shows the process of the proposed deconvolution algorithm for forward-looking scanning radar imaging with angular super-resolution. The details on this approach to find the true scene are presented next.

3. INVERSE PROBLEM

3.1. Bayesian Inversion for Deconvolution Problem

In this subsection, we convert the angular super-resolution problem into an equivalent maximum a posteriori estimation task.

Due to the lack of the high frequencies information in spatial domain, solving f by inverting (3) is highly sensitive to the noise n. To overcome this difficulty, one must utilize some prior knowledge of the true scene f. To reach this aim, we convert the angular super-resolution problem into an equivalent maximum a posteriori estimation task by using Bayesian theory, which enables us to incorporate the statistic characteristics of the prior information about the f. Bayesian methods have many advantages over other approaches, one important superiority relies in that Bayesian methods can use the statistic characteristic of the observed scene, which is often ignored by the other methods. Moreover, the Bayesian methods are model-based, they can handle observation noise and missing data problems. In Bayesian modeling, all unknowns are treated as random variables with assigned probability distribution. The idea behind the Bayesian inversion for solving (3) is that all the information about the unknowns $[f, \gamma]$ in an uncertain environment is contained in posterior law $p(f, \gamma|g)$, where f is assigned to a prior distribution $p(f, \gamma)$ with the mean equals to μ and scale equals to σ, which denotes the prior knowledge of the variable f. The observation data g is the echo data of conditional distribution $p(g|f, \gamma)$ with the mean equals to μ_n and scale equals to σ_n, which models all the information coming from the echoes and their uncertainty [15]. The set of the parameters introduced above is given by $\gamma = (\mu_f, \sigma_f, \mu_n, \sigma_n)$.

Starting from (3), the Bayesian approach for airborne forward-looking scanning radar imaging with angular super-resolution is to solve the forward model (3) by using the MAP formulation. The MAP estimation task consists of finding the solution that satisfies the following criterion:

$$f_{MAP} = \underset{f}{\operatorname{argmax}} \left[p\left(g|f, \gamma\right) p\left(f, \gamma\right) \right] = \underset{f}{\operatorname{argmin}} \left[-\ln p\left(g|f, \gamma\right) - \ln p\left(f|\gamma\right) \right]. \tag{4}$$

The solution of (4) requires the statistical characteristic of noise term and the prior of the true scene. The law to describe the statistical characteristic of the noise depends on the application. On the basic idea of radar imaging, we assume that the noise obeys the Gaussian distribution. For this reason, the Gaussian distribution with zero mean and variance equals to σ_n^2 has been introduced as a model for noise. Thus, the law for n_i can be written as

$$p\left(n_i\right) = \frac{1}{\left(\pi\sigma_n^2\right)} \exp\left[-\frac{\left(n_i\right)^2}{2\sigma_n^2} \right]. \tag{5}$$

By (4), the likelihood function f_i can be expressed as

$$p\left(g_i|f_i, \gamma_i\right) = \frac{1}{\left(\pi\sigma_n^2\right)} \exp\left[-\frac{\left(g_i - Hf_i\right)^2}{2\sigma_n^2} \right]. \tag{6}$$

Then, the likelihood function for the data f is

$$p\left(g|f, \gamma\right) = \frac{1}{\left(\pi\sigma_n^2\right)^{N_r N_a}} \exp\left[-\frac{\left\|g - Hf\right\|_2^2}{2\sigma_n^2} \right]. \tag{7}$$

where $\|\cdot\|_2$ represents the Euclidean norm.

Since the forward model of angular super-resolution includes the convolution operator, some prior information about the targets must be introduced to reduce the amplification of noise. The radar imagery demonstrates the distribution and amplitudes of the limited dominant centers of the targets, which usually represents strong sparsity [25]. Therefore, the large coefficients of scatters can capture most of the information of the scene while the weak scattering centers can be regarded as noise in radar imaging. This leads to that we focus on the sparse prior information of dominant scatterer targets in the forward-looking scanning radar imaging. The prior knowledge about the statistical characteristics of the dominant scatterers can be formulated by Laplace distribution function. The reason is that the Laplace distribution has heavy tails, which means that the probability of strong scatterers being large is

not prohibitively small [25]. On the other hand, the assumption of Laplace is motivated by the fact that it follows from concrete distributional assumptions regarding the increments in the unknown image, which can be modified to better fit the specific situation [20]. Based on the mentioned above, we use Laplace distribution to represent the scattering characteristics of targets.

Therefore, the probability density function of f could be given by

$$p\left(f,\gamma\right)=\prod_{i=1}^{N_rN_a}\frac{1}{\sqrt{2}\sigma}\exp\left[-\frac{\sqrt{2}\left|f_i\right|}{\sigma}\right]. \tag{8}$$

where f_i represents the i-th component of f and σ denotes the scale of f.

Substituting (7) and (8) into (4) and taking the logarithms to the negative log-posteriority function, the objective function of the MAP estimator could be expressed as

$$\begin{aligned} f_{MAP} &= \underset{f}{\operatorname{argmin}}\left\{\|Hf-g\|_2^2+\lambda\|f\|_1\right\} \\ \lambda &= \frac{2\sqrt{2}\sigma_n^2}{\sigma} \end{aligned} \tag{9}$$

where $\lambda>0$ is the regularization parameter, which is used to balance measurement error and prior information of the observation scene. The first term in the objective function (9) represents how well the scattering model and the estimate of the object predict the physical scattering phenomena of the true object. The second term in (9) incorporates prior information regarding the nature features of the interested scene that measures how undesirable a candidate estimates f.

The estimation criterion (9) can also be seen in a regularization perspective as a way to address the ill-posed problem of inferring f from g; in that case, $\|f\|_1$ is called the regularization function that captures the prior knowledge and λ is the regularization parameter [20].

A possible solution to compute f_{MAP} could be realized by means of classic optimization techniques whose core idea is gradient-based. However, such approaches might be ineffective when applied to solve (9). The reason results in the non-differentiability of l_1 norm around the original. To solve this problem, in what follows, a new approach called iterative shrinkage-thresholding is presented.

3.2. An Iterative Shrinkage Algorithm

In this subsection, iterative shrinkage method will be employed to solve the problem (9). We start with a review of the general framework of the iterative shrinkage algorithm.

The iterative shrinkage algorithm was initially proposed to realize the signal denoising problems in which H is identity matrix [23, 26]. In this case, the objective function (9) simplifies to

$$shrink_\lambda\left(g\right)=\underset{f}{\operatorname{argmin}}\frac{1}{2}\left\|f-g\right\|_2^2+\lambda\phi\left(f\right). \tag{10}$$

where *shrink* is the shrinkage operator defined by [24]. In this paper, we focus on $\phi(f)=\|f\|_1$, and the shrinkage operator $shrink_\lambda(g)$ is given by

$$shrink_\lambda\left(g\right)=\operatorname{sign}\left(g\right)\cdot\max\left(\left|g\right|-\lambda,0\right). \tag{11}$$

We can see that the problem (9) fits into the framework of shrinkage operator theory. So the solution of (9) can be written as:

$$f_{MAP}\in\underset{f}{\operatorname{argmin}}\left\{\frac{1}{2}\left\|Hf-g\right\|_2^2+\lambda\phi\left(f\right)\right\}. \tag{12}$$

The rationale behind the iterative shrinkage thresholding algorithm is that for any $\alpha>0$, the f_{MAP} solves the (12) if and only if the following equivalent statement holds:

$$0\in H^T(Hf_{MAP}-g)+\lambda\partial\phi(f_{MAP}) \tag{13}$$

We should note that (13) can be rewritten as

$$0\in H^T(Hf_{MAP}-g)-\alpha f_{MAP}+\alpha f_{MAP}+\lambda\partial\phi(f_{MAP}). \tag{14}$$

Moving the first two terms in (14) to the left hand of equation, then (14) becomes

$$\left[\alpha I - H^T(Hf - g)\right] f_{MAP} \in (\alpha I + \lambda \partial\phi) f_{MAP} \tag{15}$$

the solution of which is given by

$$f_{MAP} \in (\alpha I + \lambda \partial\phi)^{-1} \times \left[\alpha I - H^T(Hf - g)\right] f_{MAP} \tag{16}$$

where $\partial\phi(f)$ represents the sub-gradient of $\phi(f)$, I stands for a $(N_r \cdot N_a) \times 1$ vector of ones. The equation (13) above naturally calls for the fixed point iterative scheme.

From (16), the solution of (12) can be written as the solution of the following linear system:

$$f_{k+1} = shrink_{\lambda/\alpha}\left[f_k - \frac{1}{\alpha} H^T (Hf_k - g)\right]. \tag{17}$$

where k represents the iteration index.

The convergence of the iterative shrinkage algorithm in (17) has been established. We now recall the theorem by J. Bioucas-Dias and M. Figueiredo [23], in which convergence of the proposed deconvolution algorithm was shown. For convenience, we restate the results from [23] in the following: Let g be given by (3), where $\|f\|_1$ is convex and $\|H\|_2^2 < 2$. Let F be the set of minimum of f, which is nonempty. Fix some f_k and let the sequence $\{f_k, k \in N\}$ be produced by (17). Then $\{f_k, k \in N\}$ converges to a point $\tilde{f} \in F$.

3.3. Selection of Regularization Parameter

In this paper, angular super-resolution is performed by minimizing the (9) composed of a data fidelity term and regularization term. Super-resolution quality in such case is governed by regularization parameter that controls the weight of the prior information about the observed scene. Unfortunately, most of the referenced methods need to manually select the regularizing parameter to control the weight of the prior to guarantee the best qualitative results. To overcome this problem, several methods have been proposed to select the parameter. One approach based on the discrepancy principle is given by W. C. Karl [27]. The use of L-curve method was introduced in [28]. This method can be computationally expensive and sensitive to curvature evaluation. A generalized cross-validation (GCV) method was proposed in [29, 30]. The advantage of GCV exists in no requirement for information of noise variance.

In (9), the regularization parameter λ is used to regulate the compromise of the two terms. Note that if parameter λ is larger, the sequence generated by (17) yields an estimate with less noise, but more signal distortion. Instead, smaller λ yields an estimate with more noise, which may slow down the speed of convergence to the extreme point. Therefore, the choice of regularization parameter affects the speed of convergence and the visual quality of super-resolution results.

Equation (9) shows that the regularization parameter λ is proportional to the variance of noise and inversely proportional to the deviation of target in the illuminated scene. In practice, the accurate information about the noise σ_n and targets σ are unknown, but the statistical characteristics of those parameters may be known. Inspired by [13], we can obtain the regularization parameter λ by general statistical way. In this paper, estimation of both σ_n and σ is achieved through a maximum likelihood method. Considering that the estimation performance can be enhanced by incorporating all the observation results, the final estimation can be obtained by the average of all estimates of the observation. Then the estimation results are expressed as

$$\hat{\sigma}_n^2 = \frac{1}{N_r N_a} \sum_{i=1}^{N_r} \sum_{j=1}^{N_a} |n(\tau_i, \tau_j)|^2. \tag{18}$$

$$\hat{\sigma} = \frac{1}{M_r M_a} \sum_{i=1}^{M_r} \sum_{j=1}^{M_a} |f(x_i, y_j)|. \tag{19}$$

Noted that the value of $\hat{\sigma}_n^2$ is likely to be different under different conditions of SNR levels.

3.4. Computational Complexity

This subsection is to analyze the computational complexity of the proposed deconvolution algorithm for angular super-resolution in forward-looking scanning radar imaging. As one can see, our proposed deconvolution algorithm contains two steps, first the selection of regularization parameter and then the inner iteration. Since the update of the λ and α is fast, the computational loads of computation f_{k+1} depend on the shrink operator and the sums and the matrix-vector products by H and H^T. In this paper, operator H represents the response matrix of radar system. Therefore, the corresponding product can be computed efficiently by using the fast Fourier transform. The overall computational complexity of an iteration algorithm will depend upon the number of iterations required until the algorithm is convergent. Therefore, we only consider the computational complexity of the proposed deconvolution algorithm required by one iteration.

The computational complexity at each iteration of the proposed deconvolution algorithm involves 2 sums, 2 multiplications and 1 shrinkage operation. The cost of computing $Hf_k - g$ is $\mathcal{O}(N_aN_r(2(M_aM_r-1))) + \mathcal{O}(N_aN_r)$, while the products by H^T can be computed with $\mathcal{O}(M_aM_r(2(N_aN_r-1)))$ cost. The shrinkage operation in (17) has a linear computational complexity $\mathcal{O}(M_aM_r)$. The total number of floating-point operations required by one iteration is

$$\mathcal{O}(N_aN_r(2M_aM_r-1)) + \mathcal{O}(M_aM_r(2N_aN_r-1)) + \mathcal{O}(N_aN_r) + \mathcal{O}(M_aM_r). \tag{20}$$

Consistent with the previous notations, M_a represents the number of discrete cells in azimuth direction, M_r is the number of the discrete cells of the scene in range direction, while N_a and N_r denote the discrete point numbers along the fast and slow time dimension, respectively.

Therefore, the computational complexity is of the order $\mathcal{O}(MN)$, where M is the 1-D size of the true scene and N is the 1-D size of the echo data. It is worthy of noting that the computational complexity of the proposed method is associated with the size of echo data and the true scene. We can conclude that the computational complexity of the proposed deconvolution algorithm for forward-looking scanning radar imaging with angular super-resolution is determined by the dimensions of deconvolution problem.

4. EXPERIMENTAL RESULTS

In this section, we present experimental results with synthetic and real data to demonstrate the performance of the proposed deconvolution algorithm for angular super-resolution. Since our goal is to achieve angular super-resolution in forward-looking scanning radar imaging, we focus on the super-resolution accuracy and the noise suppression. Here, the regularization parameter λ in (17) is chosen using (18) and (19). The results are compared with those obtained by the Wiener filter.

The stopping criterion of the proposed deconvolution algorithm is that the difference between two consecutive iterates should satisfy the following inequality:

$$\|f_{k+1} - f_k\|_2 \leqslant \varepsilon. \tag{21}$$

where we use $\varepsilon = 10^{-3}$ in this section.

To quantitatively compare the angular super-resolution performance of these two algorithms, Blurred signal to noise ratio (BSNR) [31], signal-to-noise ratio (SNR), relative error (ReErr), and improved signal-to-noise ratio (ISNR) [32] are introduced. The ReErr provides a quantitative measure of the quality of the angular super-resolution result: a small ReErr value indicates that f_{MAP} is an accurate approximation of f. They are defined as follows

$$\mathrm{BSNR} = 10\log_{10}\left(\frac{\|g\|_2}{\|n\|_2}\right); \quad \mathrm{SNR} = 10\log_{10}\frac{\|f\|_2}{\|f_{MAP}-f\|_2}; \tag{22}$$

$$\mathrm{ReErr}(100\%) = \frac{\|f_{MAP}-f\|_2}{\|f\|_2}\times 100\%; \quad \mathrm{ISNR} = 10\log_{10}\frac{\|g-f\|_2^2}{\|f_{MAP}-f\|_2^2}. \tag{23}$$

where g, n, f, and f_{MAP} are the data after range compression and range cell migration, the noise vector added in the test, the original scene, and the super-resolution result, respectively. As for SNR, ReErr, and ISNR, the ideal values of those are $+\infty$, 0, and $+\infty$, respectively, and they require the existence of a true scene. Therefore, they can only be used in the simulated experiments.

We first compare the proposed deconvolution method with the Wiener filter method at different SNR levels. In all the experiments, we set the initial value to be the data after range compression and range cell migration. We also find their best regularization parameters by (18) and (19) for the smallest relative error of the super-resolution result among all the tested values.

4.1. One-dimensional Simulation Results

In this subsection, we show experimental results on synthetic data at different SNR levels to evaluate the performance of the proposed algorithm. In the first experiment, we use a synthetic scene composed of three point targets with different amplitudes that denotes scattering coefficient. The original scene is shown in Fig. 2 and the system parameters for the synthetic experiment are listed in Table 1.

In advance, the range compression and range cell migration are applied to the echo data [33]. On this basis, the echo signal is added by Gaussian white noise with SNR = 20 dB, the profile of the contaminated signal is shown in Fig. 3(a). In Fig. 3(a), the response of two closely-spaced point targets is proportional to two replicas of the antenna pattern, overlapped and added to get a composite response. In this case, the individual response is not resolved, but blur together into a single peak.

Figure 3(b) shows the angular super-resolution result of the Wiener filter. Fig. 3(c) shows the angular super-resolution result of the proposed deconvolution algorithm. In this case, the regularization parameter λ is set to be 3.2. It can be seen that these two results are nearly the same but the angular super-resolution result of the proposed method has less amplitude error than the Wiener filter. The reason is that minimum prior information about the targets is used in the Wiener filter. How ever, the Laplace distribution is used in the proposed deconvolution algorithm to represent the prior information about the statistic characteristics of the scattering coefficient of the targets.

Next, we characterize the angular super-resolution performance of the proposed deconvolution algorithm in the presence of strong noise. The same simulative scene is used as shown in Fig. 2. The range compression and range cell migration are also applied to the echo data. And the data after range compression and range cell migration are corrupted by Gaussian noise with SNR = 10 dB in this simulation, which is shown in Fig. 4(a). In this case, the regularization parameter λ is set to be 10.2.

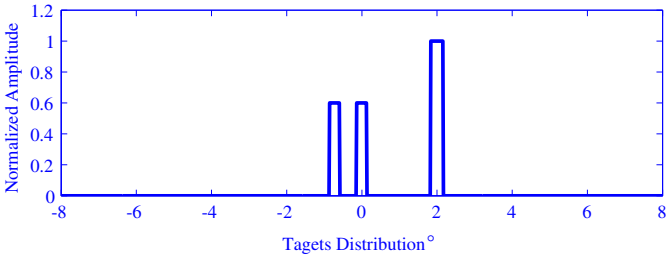

Figure 2. Location of targets in the simulate scene.

Table 1. Simulation parameters.

Parameters	Value
Carrier frequency	10 GHz
Band width	20 MHz
Pulse duration	5 μs
Pulse repetition frequency	1000 Hz
Antenna scanning velocity	30°/s
Antenna scanning area	$-8° \sim +8°$
Main-lobe beam width	3°

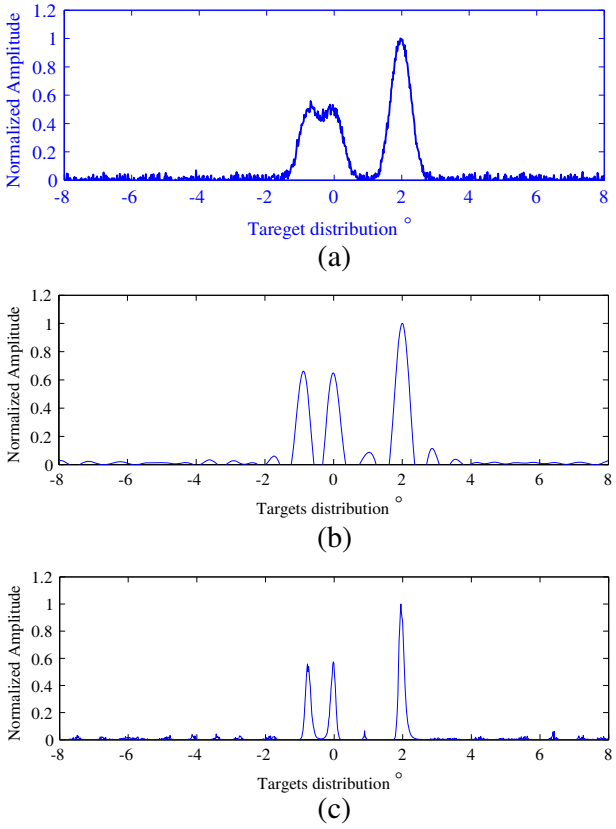

Figure 3. (a) The echo data contaminated by 20 dB noise; (b) Angular super-resolution result obtained using Wiener filter with 20 dB noise; (c) Angular super-resolution result obtained using the proposed deconvolution with 20 dB noise.

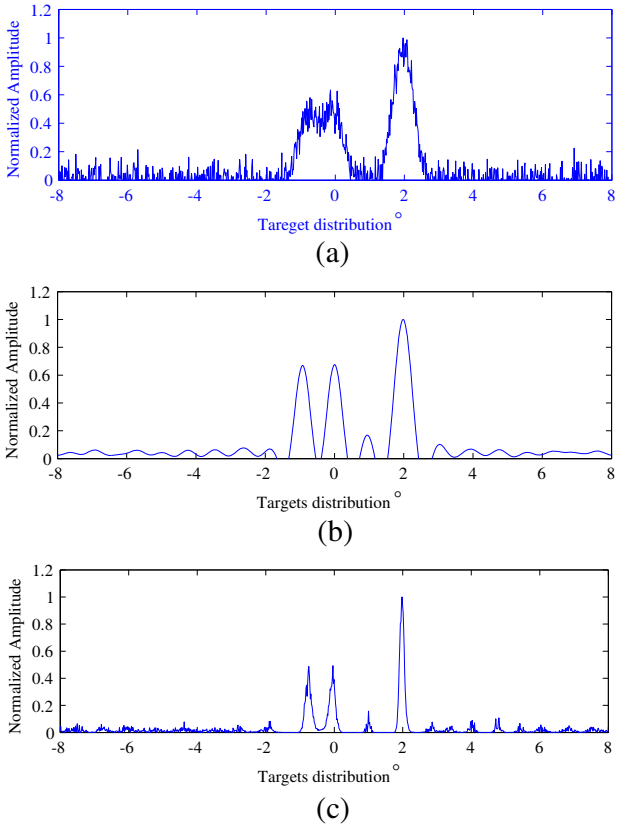

Figure 4. (a) The echo data contaminated by 10 dB noise; (b) Angular super-resolution result obtained using Wiener filter with 10 dB noise; (c) Angular super-resolution result obtained using the proposed deconvolution algorithm with 10 dB noise.

Figures 4(b) and 4(c) show the angular super-resolution result of the Wiener filter algorithm and the proposed deconvolution algorithm, respectively. It can be seen obviously that the results of angular super-resolution are rather different. The visual quality of the super-resolution result by using the proposed deconvolution method is quite competitive with the super-resolution result by using the Wiener deconvolution algorithm. From Fig. 4(c), it can be found that the proposed deconvolution approach for angular super-resolution imaging is stable in the presence of strong noise. It is obvious that the proposed deconvolution algorithm for angular super-resolution imaging can jointly estimate the amplitude of the targets and suppress the noise. However, the angular super-resolution result using Wiener filter presents worse performance in terms of noise suppression. On the other hand, due to the existence of high noise, the angular super-resolution result by using the Wiener filter is distorted apparently and several spurious peaks are shown in Fig. 4(b). Compared with the Wiener filter, the proposed deconvolution algorithm can endure noise impact in the received signal, and can keep performance of angular super-resolution at different SNR levels. Therefore, the angular super-resolution based on iterative shrinkage deconvolution has excellent stability and works well in the engineering field.

In order to quantitatively evaluate the performance of these two deconvolution algorithms for angular super-resolution. In Table 2, we compare their angular super-resolution results in terms of ISNRs, SNRs, and ReErrs, respectively. It can be seen from the table that the results of ISNRs, SNRs, and ReErrs obtained by using the proposed method are better than those by using the Wiener filter. These results demonstrate the superiority of the proposed angular super-resolution method over the Wiener filter method.

Table 2. Summary of angular super-resolution results for different methods.

Image	Method	ISNR (dB)	SNR (dB)	ReErr
Fig. 3	Wiener	−6.12	0.74	84.3%
BSNR = 5.07 dB	Proposed	−4.85	2.03	62.9%
Fig. 6	Wiener	−3.71	0.59	87.5%
BSNR = 2.56 dB	Proposed	−2.91	1.39	72.4%

The reason comes from that the Gaussian likelihood function is used to formulate the statistic characteristics of noise in the proposed deconvolution algorithm. On the other hand, the prior information of the targets is used in our deconvolution algorithm, while there is no prior information of the targets used in the Wiener filter.

4.2. Results with Real Data

To evaluate the performances of the proposed method on angular super-resolution, experimental results on real data are presented. The real data are acquired by a forward-looking scanning radar system with the center frequency in X-band. Fig. 5 shows the experimental setup of the system. The transmitted antenna pattern is obtained through the measure result in the microwave anechoic chamber in the University of Electronic Science and Technology of China. However, due to the noise and energy degradation in actual situations, the antenna pattern used in deconvolution is not consistent with the transmitted pattern. To achieve nice results, we use a pretreatment for the antenna pattern which changes the length of the sidelobe while retaining the width of the main beam of the original pattern. The width of the sidelobe is changed step by step and is chosen by the best experiment result for random data in one scan. In our experiment for scene data processing, this method for choosing the appropriate antenna pattern is effective. Some related radar parameters are listed in Table 3.

Fig. 6(a) shows the interested scene composed a ship and some buildings. The echo from the three buildings is much stronger than that from the other areas so that the scene can be considered as the combination of three point targets. The range of the center scene is 594 m and the distance between each building is about 45 m. The echo from three high buildings and the ship is stronger than that from the other areas. In this case, three buildings and the ship can be considered as distribution in a sparse way in the interested scene and this scene can also be regarded as consisting of point targets. In the experiment, three buildings and the ship capture most of the information of the interested scene. We first apply the range compression and range cell migration [33] to the echo data. The result is shown in Fig. 6(b). From Fig. 6(b), we can see that the echo of adjacent buildings is overlapping and covering the building features.

Table 3. Experimental system parameters for the real data.

Parameter	**Value**
Carrier frequency	9.6 GHz
Band width	30 MB
Sample frequency	90 MHz
Pulse duration	2 μs
Pulse repetition frequency	1000 Hz
Antenna scanning velocity	72°/s
Antenna scanning area	$-45^\circ \sim +45^\circ$
Main-lobe beam width	5.1°

Figure 5. System setup in the real experiment.

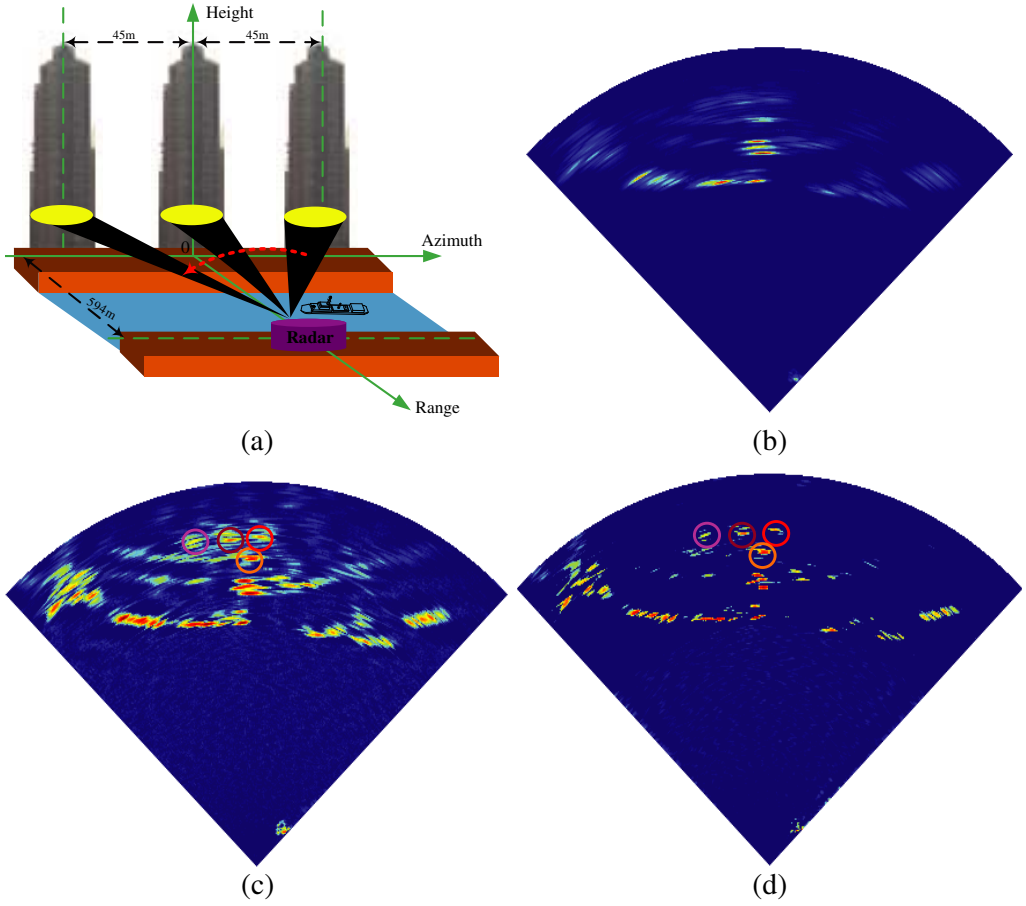

Figure 6. (a) The original scene. The horizontal and vertical direction denote the azimuth and range dimension, respectively; (b) The real-beam radar imaging after range compression and range cell migration; (c) Angular super-resolution using Wiener filter; (d) Angular super-resolution using the proposed algorithm.

Then we compare the proposed iterative shrinkage deconvolution algorithm with the conventional Wiener filter method. Fig. 6(c) shows the angular super-resolution imaging result of the Wiener filter. While Fig. 6(d) presents the angular super-resolution result of the proposed deconvolution algorithm. For the proposed deconvolution, we use the regularization parameter 2.85, and the iteration number is 36. It is obvious that the result of the proposed method has better visual effect and higher denoising

quality. This results from that the prior information of the targets in the scene of interest is adopted in the proposed deconvolution algorithm, while the Wiener filter does not contain any a priori information of the targets. The result of the real experiment proves that the proposed deconvolution algorithm is stable and accurate in angular super-resolution imaging.

5. CONCLUSION

In this paper, we propose a deconvolution algorithm for angular super-resolution imaging in forward-looking scanning radar. This approach firstly describes the angular super-resolution problem as a maximum a posteriori estimation task in the framework of Bayesian theory that is efficient in incorporating prior information of the targets. The algorithm transforms the maximum a posteriori estimation task to an equivalent unconstrained problem. It is demonstrated that the unconstrained problem can be easily solved by the iterative shrinkage method. The accuracy and the effect of our proposed deconvolution algorithm (compared with Wiener filter) in angular super-resolution imaging is verified by experiments with synthetic and real data.

As for lower SNR situations, however, the angular super-resolution performance of the proposed deconvolution algorithm is constrained, which may inhibit the usage of the proposed deconvolution algorithm in many applications. Therefore, the development of a deconvolution algorithm for angular super-resolution imaging in lower SNR situations will be our future work.

ACKNOWLEDGMENT

This work was supported by the National Natural Science Foundation of China (No. 61201272).

REFERENCES

1. Richards, M. A., J. Scheer, and W. A. Holm, *Principles of Modern Radar: Basic Principles*, SciTech Pub., 2010.
2. Ramani, S. and J. A. Fessler, "A splitting-based iterative algorithm for accelerated statistical X-ray CT reconstruction," *IEEE Transactions on Medical Imaging*, Vol. 31, No. 3, 677–688, 2012.
3. Yildirim, S., A. Cemgil, M. Aktar, Y. Ozakin, and A. Ertuzun, "A Bayesian deconvolution approach for receiver function analysis," *IEEE Transactions on Geoscience and Remote Sensing*, Vol. 48, No. 12, 4151–4163, 2010.
4. Soussen, C., J. Idier, D. Brie, and J. Duan, "From Bernoulli-Gaussian deconvolution to sparse signal restoration," *IEEE Transactions on Signal Processing*, Vol. 59, No. 10, 4572–4584, 2011.
5. Dickey, F., L. Romero, J. DeLaurentis, and A. Doerry, "Super-resolution, degrees of freedom and synthetic aperture radar," *IEE Proceedings — Radar, Sonar and Navigation*, Vol. 150, No. 6, 419–429, 2003.
6. Zha, Y., Y. Huang, and J. Yang, "Augmented lagrangian method for angular super-resolution imaging in forward-looking scanning radar," *Journal of Applied Remote Sensing*, Vol. 9, No. 1, 096055–096055, 2015.
7. Zha, Y., Y. Huang, Z. Sun, Y. Wang, and J. Yang, "Bayesian deconvolution for angular super-resolution in forward-looking scanning radar," *Sensors*, Vol. 15, No. 3, 6924–6946, 2015.
8. Tello Alonso, M., P. López-Dekker, and J. J. Mallorquí, "A novel strategy for radar imaging based on compressive sensing," *IEEE Transactions on Geoscience and Remote Sensing*, Vol. 48, No. 12, 4285–4295, 2010.
9. Gambardella, A. and M. Migliaccio, "On the superresolution of microwave scanning radiometer measurements," *IEEE Geoscience and Remote Sensing Letters*, Vol. 5, No. 4, 796–800, 2008.
10. Uttam, S. and N. A. Goodman, "Superresolution of coherent sources in real-beam data," *IEEE Transactions on Aerospace and Electronic Systems*, Vol. 46, No. 3, 1557–1566, 2010.
11. Sundareshan, M. K. and S. Bhattacharjee, "Enhanced iterative processing algorithms for restoration and superresolution of tactical sensor imagery," *Optical Engineering*, Vol. 43, No. 1, 199–208, 2004.

12. Lohner, A., "Improved azimuthal resolution of forward looking SAR by sophisticated antenna illumination function design," *IEE Proceedings — Radar, Sonar and Navigation*, 128–134, IET, 1998.
13. Xu, Z., X. Chang, F. Xu, and H. Zhang, "L1/2 regularization: A thresholding representation theory and a fast solver," *IEEE Transactions on Neural Networks and Learning Systems*, Vol. 23, No. 7, 1013–1027, 2012.
14. Ramani, S., Z. Liu, J. Rosen, J. Nielsen, and J. A. Fessler, "Regularization parameter selection for nonlinear iterative image restoration and MRI reconstruction using GCV and SURE-based methods," *IEEE Transactions on Image Processing*, Vol. 21, No. 8, 3659–3672, 2012.
15. Babacan, S. D., R. Molina, and A. K. Katsaggelos, "Variational Bayesian super resolution," *IEEE Transactions on Image Processing*, Vol. 20, No. 4, 984–999, 2011.
16. Lane, R., "Non-parametric Bayesian super-resolution," *IET Radar, Sonar and Navigation*, Vol. 4, No. 4, 639–648, 2010.
17. Richardson, W. H., "Bayesian-based iterative method of image restoration," *JOSA*, Vol. 62, No. 1, 55–59, 1972.
18. Lucy, L., "An iterative technique for the rectification of observed distributions," *The Astronomical Journal*, Vol. 79, 745, 1974.
19. White, R. L., "Image restoration using the damped Richardson-Lucy method," *The Restoration of HST Images and Spectra II*, 104–110, 1994.
20. Mohammad-Djafari, A., "Bayesian approach for inverse problems in optical coherent and noncoherent imaging," *SPIE's 48th Annual Meeting on Optical Science and Technology*, 209–218, International Society for Optics and Photonics, 2003.
21. Beck, A. and M. Teboulle, "A fast iterative shrinkage-thresholding algorithm for linear inverse problems," *SIAM Journal on Imaging Sciences*, Vol. 2, No. 1, 183–202, 2009.
22. Figueiredo, M. A. and R. D. Nowak, "An EM algorithm for wavelet-based image restoration," *IEEE Transactions on Image Processing*, Vol. 12, No. 8, 906–916, 2003.
23. Bioucas-Dias, J. M. and M. A. Figueiredo, "A new twist: Two-step iterative shrinkage/thresholding algorithms for image restoration," *IEEE Transactions on Image Processing*, Vol. 16, No. 12, 2992–3004, 2007.
24. Combettes, P. L. and V. R. Wajs, "Signal recovery by proximal forward-backward splitting," *Multiscale Modeling & Simulation*, Vol. 4, No. 4, 1168–1200, 2005.
25. Samadi, S., M. Çetin, and M. A. Masnadi-Shirazi, "Sparse representation-based synthetic aperture radar imaging," *IET Radar, Sonar and Navigation*, Vol. 5, No. 2, 182–193, 2011.
26. Donoho, D. L., "De-noising by soft-thresholding," *IEEE Transactions on Information Theory*, Vol. 41, No. 3, 613–627, 1995.
27. Karl, W. C., *Regularization in Image Restoration and Reconstruction*, Elsevier, New York, 2005.
28. Hansen, P. C., "Analysis of discrete ill-posed problems by means of the L-curve," *SIAM Review*, Vol. 34, No. 4, 561–580, 1992.
29. Zhang, Y., R. Li, and C. L. Tsai, "Regularization parameter selections via generalized information criterion," *Journal of the American Statistical Association*, Vol. 105, No. 489, 312–323, 2010.
30. Sourbron, S., R. Luypaert, P. Van Schuerbeek, M. Dujardin, and T. Stadnik, "Choice of the regularization parameter for perfusion quantification with MRI," *Physics in Medicine and Biology*, Vol. 49, No. 14, 3307, 2004.
31. Huang, Y., M. K. Ng, and Y. W. Wen, "A fast total variation minimization method for image restoration," *Multiscale Modeling & Simulation*, Vol. 7, No. 2, 774–795, 2008.
32. Figueiredo, M. A. and J. M. Bioucas-Dias, "Restoration of Poissonian images using alternating direction optimization," *IEEE Transactions on Image Processing*, Vol. 19, No. 12, 3133–3145, 2010.
33. Li, W., J. Yang, and Y. Huang, "Keystone transform-based space-variant range migration correction for airborne forward-looking scanning radar," *Electronics Letters*, Vol. 48, No. 2, 121–122, 2012.